Dalton Transactions

A Theoretical Analysis of the Phosphorescence Efficiencies of Cu(I) Complexes

Journal:	*Dalton Transactions*
Manuscript ID:	DT-ART-01-2014-000245.R1
Article Type:	Paper
Date Submitted by the Author:	23-Mar-2014
Complete List of Authors:	Zou, Lu; Institute of Theoretical Chemistry, ; Institute of Theoretical Chemistry Cheng, Yanxiang; Changchun Institute of Applied Chemistry, Chinese Academy of Sciences, State Key Laboratory of Polymer Physics and Chemistry Li, Yan; Institute of Theoretical Chemistry, Jilin University, Li, Hui; Institute of Applied Chemistry, Chinese Academy of Sciences, State Key Laboratory of Polymer Physics and Chemistry Zhang, Hong-Xing; Institute of Theoretical Chemistry, Jilin University, Ren, Ai-min; Institute of Theoretical Chemistry,

A Theoretical Analysis of the Phosphorescence Efficiencies of Cu(I) Complexes

Lu-Yi Zou,[†] Yan-Xiang Cheng,[‡] Yan Li,[†] Hui Li,[‡] Hong-Xing Zhang,[†] Ai-Min Ren[*†]

[†]State Key Laboratory of Theoretical and Computational Chemistry, Institute of Theoretical Chemistry, Jilin University, Changchun 130023, P. R. China

[‡]State Key Laboratory of Polymer Physics and Chemistry, Institute of Applied Chemistry, Chinese Academy of Sciences, Changchun 130022, P. R. China.

*Corresponding author. E-mail addresses: aimin_ren@yahoo.com.

Fax: +86 431 88498567

Abstract: We herein report a theoretical analysis using density functional theory (DFT) and time-dependent DFT (TDDFT) to study the electronic structures and photophysical properties of mixed-ligand Cu(I) complexes. The evaluation of the non-radiative and radiative decay rate constants (k_{nr} and k_r) is presented. It is found that large SOC matrix elements are not necessarily result in the large k_r. Introducing POP (bis[2-(diphenylphosphino)phenyl]ether) ligand compared with a pair of PPh_3 (triphenylphosphine) ligands, the ether linkage plays an important role in governing the quantum efficiency of the studied complexes. However, the balance between hole injection and electron acceptance, which leading to the quantum yield of $[Cu(dmp)(POP)]^+$ further towards $[Cu(dbp)(POP)]^+$, is another important factor in tuning the quantum efficiency. A thorough understanding of the effect of the

coordinating ligand on the photophysical behavior of a transition metal complex is desirable for rational syntheses of highly phosphorescent materials.

1. Introduction

Phosphorescent organic light emitting diodes (OLEDs) possess advantages over fluorescent ones because strong SOC interactions to effect facile intersystem crossing (ISC) and fast k_r, which can weaken the spin-forbiddenness of the electronic transitions between T_1 and S_0 [1]. However, most known efficient phosphorescent emitters are containing Ir(III), Pt(II) or other rare earth metals, which are highly costs and environmental concerns result in inherent limitations [2-4]. From economical viewpoint, developing of phosphorescent complexes containing non-precious metals is desired in terms of cost effectiveness and a stable supply of phosphorescent guest molecules. An attractive alternative is emerging, Cu(I) complexes present the same photophysical characteristics compare to Ru（II) metal complexes [5-7], consist of non-toxic, inexpensive, and environmentally safe.

Thanks to McMillin and co-workers [8-12], which have accomplished much of the pioneering work with Cu(I) compounds. One of the pivotal works in solution is well established [13], their photoluminescence quantum yield in methylene chloride has been greatly improved, up to 0.16, by using an ether bridged phosphine ligand and a phenanthroline ligand with bulky substituents. The structure-property relationship are observed from the X-ray diffraction and the prediction of stokes shift in experimental [14]. Theoretical investigation becomes indispensable to obtain the excited state structure and the origin of the emission, which are still ambiguous. The aim of the

present work is to provide an in-depth understanding of the optical and electronic properties of these complexes, and to provide some useful information for the experimentalist.

2. Computation methods

Geometric and electronic structures of the considered complexes, as well as their cationic and anionic structures, were fully optimized by DFT using the B3LYP hybrid functional combined with the 6-31G(d) basis set except Cu. The quasi-relativistic pseudopotentials of Cu proposed by Hay and Wadt with 19 valence electrons were employed, and a "double-ξ" quality basis set LANL2DZ was adopted as the basis set [15-17]. The lowest singlet (S_1) and triplet excited geometries were computed by TDDFT and DFT with the B3LYP and unrestricted B3LYP (UB3LYP), respectively. Full geometry optimizations without symmetry constraints were carried out in the gas phase for the singlet ground state, the lowest singlet and triplet excited states. Following these states optimization, the vibrational frequencies were calculated and the results showed that all optimized structures are stable geometric structures. The absorption and emission wavelengths of these complexes were systematically investigated by employing TDDFT method. The influence of solvent DCM on the absorption and emission spectra of these complexes was simulated by using the Polarizable Continuum Model (PCM). All of calculations of these studied complexes in this work have been performed with Gaussian 09 program package [18].

3. Results and Discussion

3.1. Geometry Optimization

The sketch maps of the studied complexes are depicted in Fig. 1, and the optimized S_0 and T_1 structures of these complexes are plotted in Fig. 2. The selected important bond lengths and angles, and dihedral angle (DHA) between the planes N-Cu-N and P-Cu-P of these complexes in both the S_0 and T_1 states are listed in Table 1, associated with data from the X-ray structure. The results show that the adopted basis set and functional can reflect the change trend of the optical and electronic properties.

The calculated bond lengths of S_0 are longer than the data from experimental X-ray structures [12, 13], the reason is the calculations are carried out in isolated gas phase lacking of crystal packing forces. From the present S_0 and T_1 states analysis, most Cu-P and Cu-N distances of $[Cu(NN)(POP)]^+$ are shorter than those of $[Cu(NN)(PPh_3)_2]^+$. It is means that the POP ligand is in closer proximity to the center metal than the PPh_3 ligand due to the ether linkage. The strengthened metal-ligand interaction will increase the probability of charge transfer from metal to the ligand. Another potentially important consequence of the ether linkage is that the P-Cu-P angle of S_0 state decreases from 124.73-125.93° in the system PPh_3 to 113.92-117.97° in system POP. It suppresses the formation of five-coordinate of the $[Cu(NN)(POP)]^+$ complexes (see Fig. 2), which is important to improve thermal stability. Moreover, it is usually known that the closer the structures between S_1 and T_1 states, the faster the corresponding ISC rate will be. The system POP has smaller bond length changes between S_1 and T_1 states than that of system PPh_3 due to the ether linkage keeping stronger rigidity structure. It is an efficient way that introduction of POP ligand primarily influences the photophysical properties via the ether linkage which

strengthen the metal-ligand interaction to improve the thermal stability, and consequently to enhance the phosphorescent quantum efficiency. Furthermore, the thermal vibrational energy of T_1 state is obtained to further investigate the intramolecular interactions, which are 470.2, 506.9 and 618.4, and 481.6, 516.6 and 629.6 kcal mol^{-1} for the POP and a pair of PPh_3 ligands in phen, dmp and dbp, respectively. The results in system POP are all lower about 10 kcal mol^{-1} than that of system PPh_3. The ether linkage indeed reduces the vibrational effects involving in POP ligand modes. Thus, the strengthened metal-ligand interaction via the ether linkage is a critical factor to increase the metal-to-ligand charge transfer (MLCT) character, which may be the origin of the high efficiency of these $[Cu(NN)(POP)]^+$ complexes.

For system POP, the geometry changes between S_0 and T_1 states in phen, dmp and dbp are gradually reduced as the substituents on the NN moiety become longer (the average change of the important bond length and angle, which are listed in Table 1, for phen, dmp and dbp are 0.1329, 0.1279 and 0.0086 Å, and 16.56, 7.26 and 0.69°, respectively), especially the unbond Cu…O distance and the DHA (the unbond Cu…O distance and the DHA for phen, dmp and dbp are 0.2037, 0.0968 and 0.0177 Å, and 28.41, 12.22 and 0.49°, respectively). The bulky substituents can sterically inhibit structural distortion from S_0 to T_1 state, which may narrow stokes shift, and therefore depress non-radiative decay.

In addition, the Cu-P bond lengths are lengthened, but Cu-N are shortened from S_0 to T_1 state in these complexes. It means that the electronic cloud distribution of

HOMO will be localized on a pair of PPh_3 or the POP ligands, the LUMO will be localized on NN moiety. The ligand-to-ligand charge transfer (LLCT) must be participated in the transition obviously. It will be proved by the following section immediately.

3.2. Frontier Molecular Orbitals

The HOMO and LUMO energies, the HOMO-LUMO gaps (Δ_{H-L}), and the lowest singlet excited energies (E_{S1}) of these complexes are listed in Table 2. The HOMO and LUMO values in system POP are all higher than each of system PPh_3, but LUMO values remain below -4.0 eV. It indicates that the hole injection ability are enhanced by the ether linkage, while the electron injection barrier is still lower (variation is not more than 0.06 eV). The Δ_{H-L} obtained by DFT is larger than the E_{S1} values from TDDFT calculations [19]. It could be ascribed to the neglect of interelectronic interaction upon the single one-electron excitation in estimating Δ_{H-L}. Although there are discrepancies between the computed Δ_{H-L} and E_{S1}, the variation trend in system PPh_3 and POP is similar. The energy gaps for Δ_{H-L} and E_{S1} in system PPh_3 and POP increase in the order of phen, dmp and dbp. We predict that the emission spectra in system PPh_3 and POP are expected to be gradually blue-shifted with the order.

The maps of the frontier orbitals of these complexes by GaussView are plotted in Fig. 3. It is noted that the electronic cloud distribution of HOMO in these complexes are mainly localized on 3d of Cu (>32%, see Table S1), and the POP or a pair of PPh_3 ligands, while the LUMO are largely localized on the NN moiety. The more detailed contributions for Cu atom of these complexes at S_0 state in solvent DCM were shown

in Table S2. The HOMO mainly possesses Cu d-orbital character, which is arising from d_{xy} and d_{x2-y2} orbital in system PPh_3 and POP for phen and dmp, respectively. However, the Cu d-orbital character in HOMO is predominantly contributed by d_{yz} and d_{xz} orbital for $[Cu(dbp)(PPh_3)_2]^+$, d_{z2} orbital for $[Cu(dbp)(POP)]^+$, respectively. The contribution of Cu atom to HOMO increases by the ether linkage and the volume of substituents on R increasing. The electronic absorption transitions of these complexes primarily arise from the mixing of MLCT and LLCT.

3.3. Absorption Spectra in DCM Solvent

Simulated absorption spectra (Fig. 4) of these complexes in DCM solvent show that systems PPh_3 and POP have similar shape of absorption curves. The lowest $S_0 \rightarrow S_1$ has the largest oscillator strengths in these complexes, which mainly promote an electron from HOMO to LUMO (Table 3). The oscillator strengths of the absorption maximum in system POP are all higher than that in system PPh_3.

The maximum absorption spectra and the experimental in system POP for phen, dmp and dbp are 403.8, 393.8 and 383.8 nm, and 391, 383 and 378 nm, respectively [13]. It is consistent with the experimental values, and the values of both calculated and experimental have the same sequence in blue-shifted. However, the absorption spectra in system PPh_3 [13], which is in accord with the experiments are assigned to the $S_0 \rightarrow S_4$ and $S_0 \rightarrow S_3$ electronic transition, mainly come from the excitations of HOMO-1 to LUMO for phen, and dmp and dbp, respectively. All these transitions are attributed to MLCT and LLCT character [d(Cu) + π(PPh_3/POP ligand) $\rightarrow$ π^*(NN moiety)] (Table S2). The results confirm that the prediction from section 3.1.

3.4. Phosphorescence

The emission spectra peaks in DCM media (Table 4) and in gas-phase (Table S3) are red shift with respect to the experimental data by 43.1-72.2 and 47.1-154.4 nm, respectively [13]. The solvent impact on phen is the greatest due to without the substitute on R. Although they deviate away from the experimental values, the TDDFT/DFT method correctly reflects the change trend of the optical and electronic properties. Table 4 shows that all the calculated emissions originate mainly from HOMO or HOMO-1 to LUMO (>46%), which is mainly composed by mixed MLCT/LLCT (Table S4).

Furthermore, the 0-0 and T_1-S_0 vertical transition energies of these complexes are obtained on the basis of the present DFT results without the solvent effect. The 0-0 transition takes into account the zero-point energies (zpe) of both the optimized S_0 and T_1 states geometries. The T_1-S_0 vertical transition energies is the difference between the T_1 and S_0 states at the T_1 optimized geometries, as shown in Fig. 6. In general, the 0-0 transition energies are higher than the experimental data, whereas the T_1-S_0 vertical transition energies are in well agreement with the experimental data (Table 5). In addition, compared with our studied complexes, the **[**Cu(dbp)(POP)]$^+$ has the smallest stokes shift to research the phosphorescence spectrum.

3.5. The Phosphorescence Quantum yields of System POP

The Φ_p can be expressed as Eq. (1):

$$\phi_p = \frac{k_r}{k_r + k_{nr}} \quad (1)$$

The k_{nr} from the T_m to the S_0 states is usually expressed in the form of the energy law Eq. (2) [20], and the k_r is given by Eq. (3) [21, 22]:

$$k_{nr}(T_m \rightarrow S_0) \propto \exp\left\{-\beta\left[E(T_m) - E(S_0)\right]\right\} \quad (2)$$

$$k_r(T_m \rightarrow S_0) = \frac{\eta^3 E(T_m)^3}{1.5}\left\{\sum_n \frac{\left\langle T_m \left| \hat{H}_{SOC} \right| S_n \right\rangle}{E(S_n) - E(T_m)} \times \left(\frac{f_n}{E(S_n)}\right)^{1/2}\right\}^2 \quad (3)$$

$$H_{SOC} = \sum_i \frac{1}{4\pi\varepsilon_0} \frac{Ze^2}{2m_e^2 c^2} \frac{1}{r^3} l_i s_i \quad (4)$$

where $\left\langle T_m \left| \hat{H}_{SOC} \right| S_n \right\rangle$ present the SOC matrix elements in $T_m \rightarrow S_n$ transition, η, $E(T_m)$, $E(S_n)$, and f_n are the refractive index of the medium (the refractive index η of DCM solution is taken to be 1.424), the energy of the *m*th triplet and *n*th singlet states, and oscillator strength, respectively.

In other words, the excited-state wavefunction ($^{1,3}\Psi$) obtained by TDDFT is expressed as a linear combination of one-electron excitation configurations ($^{1,3}\psi_i$) from an occupied molecular orbital to an unoccupied molecular orbital (eg. From HOMO to LUMO):

$$^{1,3}\Psi = \sum_i a_i \, ^{1,3}\psi_i \quad (5)$$

where a_i is the coefficient of the configuration $^{1,3}\psi_i$ to the excited-state wavefunction $^{1,3}\Psi$.

The molecular orbitals (ψ_i) can be expanded using natural atomic orbitals (χ_k):

$$\psi_i = \sum_k c_{ki} \chi_k \quad (6)$$

where c_{ki} is the coefficient of AO χ_k to MO ψ_i.

The one-electron one-center spin-orbit integral is non-vanishing only when the T_m and S_n states involve the same unoccupied π^* orbital but different occupied d orbitals.

Then the SOC matrix elements $\left\langle \mathrm{T_m}\left|\hat{H}_{SOC}\right|\mathrm{S_n}\right\rangle$ can be written as follows [23]:

$$\begin{aligned}\left\langle {}^3\Psi_{\mathrm{m}}\left|\hat{H}_{SOC}\right|{}^1\Psi_{\mathrm{n}}\right\rangle &= \left\langle \sum_i {}^3a_i\,{}^3\psi_l\left|H_{SOC}\right|\sum_j {}^1a_j\,{}^1\psi_j\right\rangle \\ &= \left\langle \sum_i {}^1a_i\left(\sum_k c_{ki}\,{}^3\left(d_{ki}\pi^*\right)\right)\left|\hat{H}_{SOC}\right|\sum_j {}^1a_j\left(\sum_l c_{lj}\,{}^1\left(d_{lj}\pi^*\right)\right)\right\rangle\end{aligned} \quad (7)$$

In which, the spin-orbit integrals $\left\langle {}^3\psi_l\left|\hat{H}_{SOC}\right|{}^1\psi_j\right\rangle$ can be proximately expressed as follows [24]:

$$\left\langle {}^3\psi_l\left|\hat{H}_{SOC}\right|{}^1\psi_j^*\right\rangle = \zeta_c\left\langle {}^3d_{ki}\pi\left|\hat{l}\hat{s}\right|{}^1d_{lj}\pi\right\rangle \quad (8)$$

$\hat{l}$ and $\hat{s}$ are angular momentum operators for orbital and spin, and ζ_c presents the one-electron spin-orbit coupling constant of the d orbital, respectively. The ζ_c value for the 3d electron of Cu is equal to 829 cm^{-1} [21]. And the matrix elements $\left\langle {}^3d_{ki}\pi^*\left|\hat{l}\hat{s}\right|{}^1d_{lj}\pi^*\right\rangle$ are listed in Table S5 [22].

Due to the signs of the coefficients of the configuration ${}^{1,3}\psi_i$ to the excited-state wavefunction ${}^{1,3}\Psi$ (a_i) obtained by TDDFT, the $\left\langle \mathrm{T_m}\left|\hat{H}_{SOC}\right|\mathrm{S_n}\right\rangle$ matrix elements can be positive or negative according to Equation (7). As being considered in Equations (3) and (7), two large SOC matrix elements may be result in small k_r results if they are of opposite signs and cancel each other out, and the k_r is always positive, since it is proportional to the square of the SOC matrix elements.

To reflect more accurately the phosphorescence properties, the SOC matrix elements and k_r by the Equations (3), (7) and (8) were calculated (listed in Tables S6-S11). The k_r follow the order: dbp ($(T_1\rightarrow S_0) = 7.95\times10^2\ s^{-1}$) > dmp ($(T_1\rightarrow S_0) = 3.64\times10^2\ s^{-1}$) > phen ($(T_1\rightarrow S_0) = 3.03\times10^2\ s^{-1}$).

From Eq. 2, the k_{nr} of an excited state increases as the energy difference between the *m*th triplet excited state and the singlet ground state decreases [23]. The energy gap law $E(T_1\text{-}S_0)$ of phen, dmp and dbp are 57.84, 61.62 and 64.04 kcal mol^{-1}, respectively. Additionally, the k_{nr} decreases with β decreasing (see section 3.1). Considering the two factors, the order of k_{nr} is phen > dmp > dbp.

From the above discussion, it can be concluded that the photoluminescent quantum efficiency following the order: dbp > dmp > phen. This is consistent with the experiments.

Furthermore, we suggest that the difference in their Φ_p were due to the stronger metal-ligand interaction in system POP compared with that in PPh_3. Take one of compounds in system PPh_3 for example, the k_r of $[Cu(dmp)(PPh_3)_2]^+$ ($(T_2 \rightarrow S_0)$ = 0.23×10^2 s^{-1}, Tables S12-13) is much smaller than anyone in that of system POP. The result confirms our previous conclusion from section 3.1 discussion above.

3.6. Comparison of Performance in OLEDs

For OLEDs emissive layer material, low injection energy barrier and transport balance of charge carrier are very important issue. The IP and EA are well-defined properties that can be calculated by DFT to estimate the energy barrier for the injection of both holes and electrons into the complexes. The calculated IPs, EAs, both vertical (v; at the geometry of the neutral complex) and adiabatic (a; optimized structure for both the neutral and charged complex), and the extraction potentials (HEP and EEP for the hole and electron, respectively) that refer to the geometry of the ions are listed in Table 6. All the IP(a) and EA(a) values in system POP are lower than

that of system PPh_3, respectively. It means that the ability of the hole injection is dramatically improved by the ether linkage, which demonstrates the prediction in the HOMO energies discussion earlier.

At the microscopic level, the charge transport mechanism in thin film can be described as a self-exchange transfer process, in which an electron or hole transfer occurs from one charged molecule to an adjacent neutral molecule. The rate of intermolecular charge transfer (K_{et}) can be estimated from Marcus theory [25] given in

$$K_{et} = A\exp\left[\frac{-\lambda}{4k_bT}\right] \quad (9)$$

where A is a prefactor related to the electronic coupling between adjacent molecules, λ is the reorganization energy, and k_b is the Boltzmann constant, T is the temperature. It will be seen that variations in the reorganization energies, which are exponential component (Eq. 9), dominate the changes in overall carrier transfer rates as the molecular structures are varied. For efficient charge transport, the reorganization energy requires to be small. At this stage, our discussion focuses on the reorganization energy.

The λ value is generally determined by fast changes in molecular geometry (the inner reorganization energy λ_i) and by slow variations in solvent polarization of the surrounding medium (the external contribution λ_e). In the case of LEDs (there are condensed-state systems), however, the latter contribution is much smaller than the former, so that the former becomes the dominant factor. The calculation method of the

inner reorganization energy λ_i for hole and electron transfer is same as our previous used one in reference [26]

The calculated λ_{hole} and $\lambda_{electron}$ are also listed in Table 6. The lower the λ value, the higher the charge transport rate. Furthermore, the balance between hole injection and electron acceptance is required as emitting-layer materials. The difference between the λ_{hole} and $\lambda_{electron}$ for $[Cu(dbp)(PPh_3)_2]^+$, $[Cu(dmp)(POP)]^+$ and $[Cu(dbp)(POP)]^+$ is less than 0.10 eV, implying that they will be better emitter with high quantum efficiency than others. The rank of the transport balance of these complexes is $[Cu(dmp)(POP)]^+$ (0.03 eV) > $[Cu(dbp)(POP)]^+$ = $[Cu(dbp)(PPh_3)_2]^+$ (0.08 eV) > $[Cu(dmp)(PPh_3)_2]^+$ (0.12 eV) > $[Cu(phen)(POP)]^+$ (0.24 eV) > $[Cu(phen)(PPh_3)_2]^+$ (0.25 eV). It shows that the bulky substituents on R can improve the transport equilibrium property evidently.

An improved understanding of ligand modification effect on photophysical properties is important in the rational search for new metal complexes. The results present here demonstrate that k_r of $[Cu(phen)(POP)]^+$ (3.03×10^2 s^{-1}) and $[Cu(dmp)(POP)]^+$ (3.64×10^2 s^{-1}) are relatively small compared with that of $[Cu(dbp)(POP)]^+$ (7.95×10^2 s^{-1}). Meanwhile, the k_{nr} gradually gets smaller from $[Cu(phen)(POP)]^+$ to $[Cu(dmp)(POP)]^+$ and then to $[Cu(dbp)(POP)]^+$ from qualitative comparison. According to the Eq. 1, the quantum yield of $[Cu(dmp)(POP)]^+$ will be significantly lower than that of $[Cu(dbp)(POP)]^+$, nearly to that of $[Cu(phen)(POP)]^+$. However, it is contrary in experiments ($[Cu(phen)(POP)]^+$ of Φ_p = 0.0018, $[Cu(dmp)(POP)]^+$ of Φ_p = 0.15, and $[Cu(dbp)(POP)]^+$ of Φ_p = 0.16). We think the key

factor is that the $[Cu(dmp)(POP)]^+$ has better transport balance than two of them, i.e. its exciton formation probability is high in OLEDs. It suggests that grafting CH_3 and $(CH_2)_3CH_3$ onto R is an efficient way to enhance the quantum yield for OLED materials.

4. Conclusions

In this study, the geometries, electronic structures, photophysical properties and phosphorescence efficiencies of these complexes were investigated by DFT and TDDFT methods. According to the geometry optimization analysis, the calculation of the thermal vibrational energy of T_1 and k_r, and the qualitative comparison of k_{nr}, it is concluded that the ether linkage indeed enhances the coordination interaction between Cu and ligands in system POP and reduces the vibrational effects. This may be the origin of the POP ligand as a stronger emitter than that a pair of PPh_3 ligands. However, the comparison of performance in OLEDs suggests that $[Cu(dmp)(POP)]^+$ and $[Cu(dbp)(POP)]^+$ are better emitter with high quantum efficiency than others, the bulky substituents on R besides sterically inhibiting structural distortion from S_0 to T_1 state and narrowing stokes shift thus depressing non-radiative decay, the improvement of the transport balance of charge carrier also is a noteworthy reason. It will be both interesting and important to consider how ligand effects influence the quantum efficiency of this kind of complexes.

Acknowledgments

This work is supported by the National Natural Science Foundation of China (Nos. 20973078, 21173099, 20874098 and 51073152), the National Basic Research

Program of China (973 Program) (No. 2013CB834801), and the Cutting-edge Science and Interdisciplinary Innovation Projects of Jilin University.

Appendix A. Supplementary data

Supplementary data associated with this article can be found.

References

[1] R. Czerwieniec, J. Yu, H. Yersin, Inorg. Chem. 50 (2011) 8293-8301.

[2] M.A. Baldo, D.F. O'Brien, Y. You, A. Shoustikov, S. Sibley, M.E. Thompson, S.R. Forrest, Nature 395 (1998) 151.

[3] C. Adachi, M.A. Baldo, M.E. Thompson, S.R. Forrest, J. Appl. Phys. 90 (2001) 5048-5051.

[4] Y.L. Tung, S.W. Lee, Y. Chi, Y.T. Tao, C.H. Chien, Y.M. Cheng, P.T. Chou, S.M. Pengc, C.S. Liud, J. Mater. Chem. 15 (2005) 460–464.

[5] R.A. Rader, D.R. McMillin, M.T. Buckner, T.G. Matthews, D.J. Casadonte, R.K. Lengel, S.B. Whittaker, L.M. Darmon, F.E. Lytle, J. Am. Chem. Soc. 103 (1981) 5906-5912.

[6] D.V. Scaltrito, D.W. Thompson, J.A.O'Callaghan, G.J. Meyer, Coord. Chem. Rev. 208 (2000) 243–266.

[7] N. Armaroli, Chem. Soc. Rev. 30 (2001) 113–124.

[8] D.R. McMillin, K.M. McNett, Chem. Rev. 98 (1998) 1201.

[9] M.T. Buckner, D.R. McMillin, J. Chem. Soc. Chem. Commun. (1978) 759-761.

[10] D.R. McMillin, M.T. Buckner, B.T. Ahn, Inorg. Chem. 16 (1977) 943.

[11] J.R. Kirchhoff, D.R. McMillin, W.R. Robinson, D.R. Powell, A.T. McKenzie, S. Chen, Inorg. Chem. 24 (1985) 3928-3933.

[12] C.E.A. Palmer, D.R. McMillin, Inorg. Chem. 26 (1987) 3837-3840.

[13] D.G. Cuttell, S.M. Kuang, P.E. Fanwick, D.R. McMillin, R.A. Walton, J. Am. Chem. Soc. 124 (2002) 6-7.

[14] Q. Zhang, Q. Zhou, Y. Cheng, L. Wang, D. Ma, X. Jing, Adv. Mater. 16 (2004) 432-436.

[15] P.J. Hay, W.R. Wadt, J. Chem. Phys. 82 (1985) 270.

[16] W.R. Wadt, P.J. Hay, J. Chem. Phys. 82 (1985) 284.

[17] P.J. Hay, W.R. Wadt, J. Chem. Phys. 82 (1985) 299.

[18] M.J. Frisch, G.W. Trucks, H.B. Schlegel, G.E. Scuseria, M.A. Robb, J.R. Cheeseman, G. Scalmani, V. Barone, B. Mennucci, G.A. Petersson, H. Nakatsuji, M. Caricato, X. Li, H.P. Hratchian, A.F. Izmaylov, J. Bloino, G. Zheng, J.L. Sonnenberg, M. Hada, M. Ehara, K. Toyota, R. Fukuda, J. Hasegawa, M. Ishida, T. Nakajima, Y. Honda, O. Kitao, H. Nakai, T. Vreven, J.A. Montgomery, Jr., J.E. Peralta, F. Ogliaro, M. Bearpark, J.J. Heyd, E. Brothers, K.N. Kudin, V.N. Staroverov, R. Kobayashi, J. Normand, K. Raghavachari, A. Rendell, J.C. Burant, S.S. Iyengar, J. Tomasi, M. Cossi, N. Rega, J.M. Millam, M. Klene, J.E. Knox, J.B. Cross, V. Bakken, C. Adamo, J. Jaramillo, R. Gomperts, R.E. Stratmann, O. Yazyev, A.J. Austin, R. Cammi, C. Pomelli, J.W. Ochterski, R.L. Martin, K. Morokuma, V.G. Zakrzewski, G.A. Voth, P. Salvador, J.J. Dannenberg, S. Dapprich, A.D. Daniels, O. Farkas, J.B. Foresman, J.V. Ortiz, J. Cioslowski, D.J. Fox, Gaussian 09, Revision A.02, Gaussian, Inc., Wallingford CT, 2009.

[19] G.R. Hutchison, M.A. Ratner, T.J. Marks, J. Am. Chem. Soc. 127 (2005) 2339.

[20] J. S. Wilson, N. Chawdhury, M. R. A. Al-Mandhary, M. Younus, M. S. Khan, P. R. Raithby, A. Köhler, R. H. Friend, J. Am. Chem. Soc. 123 (2001) 9412-9417.

[21] Z.A. Siddique, Y. Yamamoto, T. Ohno, K. Nozaki, Inorg. Chem. 42 (2003) 6366-6378.

[22] T. Azumi, H. Miki in Spectroscopy of the Spin sublevels of Transition Metal Complexes (Ed. H. Yersin), Springer Berlin Heidelberg, (1997).

[23] G.S. Tong, C.M. Che, Chem . Eur. J. 15 (2009) 7225.

[24] A.F. Rausch, H.H. Homeier, P.I. Djurovich, M.E. Thompson, H. Yersin in Spin-orbit coupling routes and OLED performance-Studies of blue-light emitting Ir (III) and Pt (II) complexes (Ed.: H. Zakya, Kafafi, S. Frank), (2007) 66550F.

[25] R.A. Marcus, Rev. Mod. Phys. 65 (1993) 599.

[26] L.Y. Zou, M. S. Ma, Z. L. Zhang, H. Li, Y. X. Cheng, A. M. Ren, Org. Electron. 13 (2012) 2627-2638.

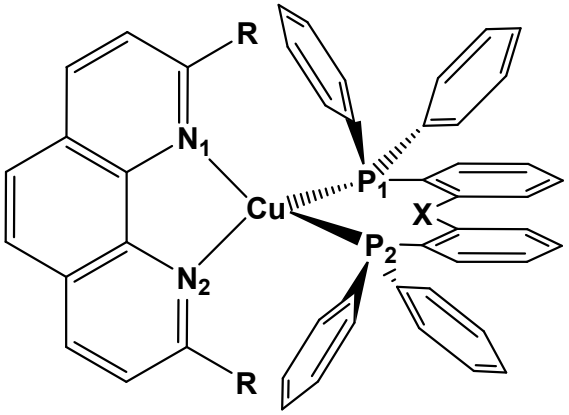

X=H,H;

R=H, $[Cu(phen)(PPh_3)_2$

R=CH_3, $[Cu(dmp)(PPh_3)_2]^+$

R=$(CH_2)_3CH_3$, $[Cu(dbp)(PPh_3)_2]^+$

X=O;

R=H, $[Cu(phen)(POP)]^+$

R=CH_3, $[Cu(dmp)(POP)]^+$

R=$(CH_2)_3CH_3$, $[Cu(dbp)(POP)]^+$

Fig. 1. Sketch map of the studied structures.

$[Cu(phen)(PPh_3)_2]^+$	$[Cu(dmp)(PPh_3)_2]^+$	$[Cu(dbp)(PPh_3)_2]^+$	$[Cu(phen)(POP)]^+$	$[Cu(dmp)(POP)]^+$	$[Cu(dbp)(POP)]^+$
Ground State S_0					
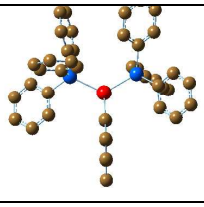	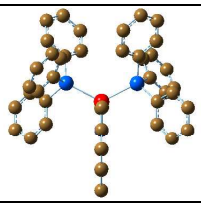	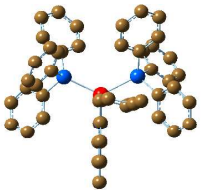	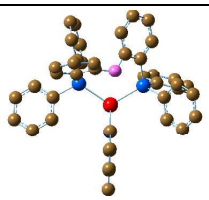	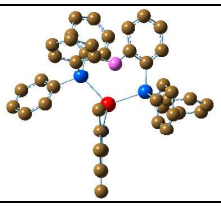	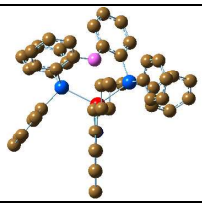
Excited State T_1					
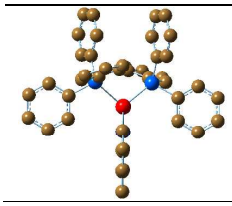	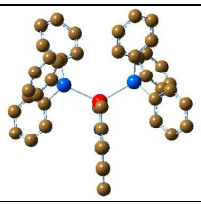	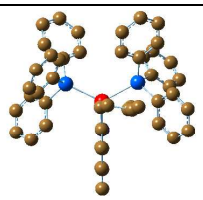	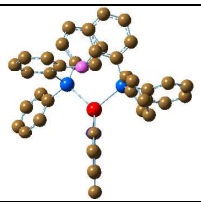	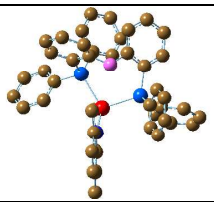	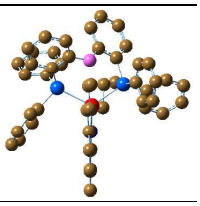

Fig. 2. The optimized S_0 and T_1 structures of these complexes.

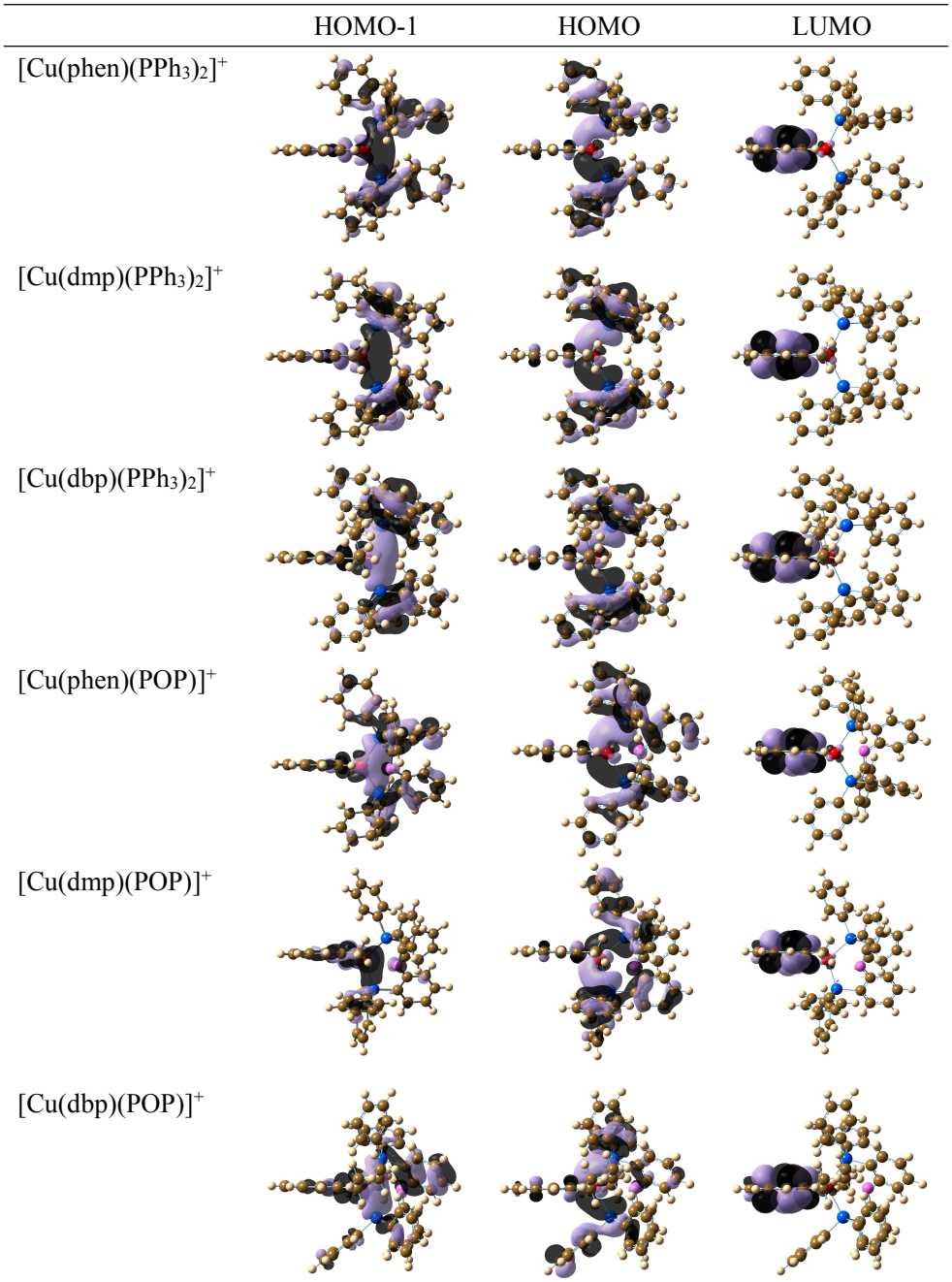

Fig. 3. Electronic density contours of the frontier orbitals for these complexes.

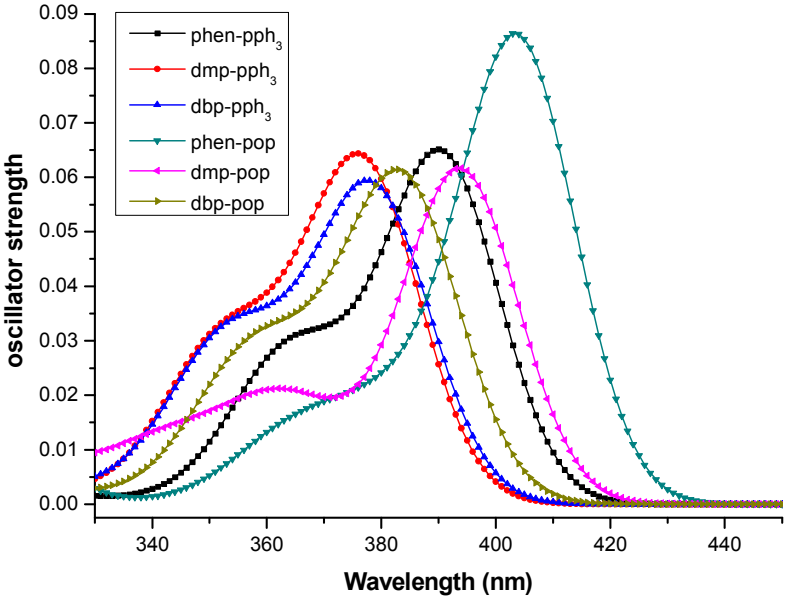

Fig. 4. Simulated absorption spectra of these complexes in DCM solution.

Table 1. Selected Bond Lengths (Å), Bond Angles (°), and Dihedral Angle (°) at Optimized S_0, S_1 and T_1 Geometries for these Complexes

	$[Cu(phen)(PPh_3)_2]^+$			$[Cu(dmp)(PPh_3)_2]^+$				$[Cu(dbp)(PPh_3)_2]^+$			$[Cu(phen)(POP)]^+$				$[Cu(dmp)(POP)]^+$				$[Cu(dbp)(POP)]^+$			
	S_0	S_1	T_1	S_0	Expt.[a]	S_1	T_1	S_0	S_1	T_1	S_0	Expt.[b]	S_1	T_1	S_0	Expt.[b]	S_1	T_1	S_0	Expt.[b]	S_1	T_1
Cu-N_1	2.1873	2.0786	2.0245	2.2012	2.105	2.0685	2.1877	2.2129	2.0790	2.2023	2.1765	2.064	2.0650	2.0213	2.2017	2.104	2.1128	2.0764	2.1885	2.109	2.1216	2.1714
Cu-N_2	2.2017	2.0852	2.0250	2.2012	2.129	2.0683	2.1877	2.2019	2.0595	2.1952	2.1759	2.071	2.0772	2.0028	2.1920	2.084	2.0464	2.0006	2.1768	2.097	2.0428	2.1669
Cu-P_1	2.3850	2.5488	2.4751	2.4122	2.305	2.5390	2.4165	2.4272	2.5611	2.4275	2.3702	2.231	2.4966	2.4760	2.4277	2.269	2.5985	2.5455	2.3928	2.271	2.6164	2.3956
Cu-P_2	2.3786	2.4717	2.4759	2.4122	2.282	2.5377	2.4165	2.4173	2.5579	2.4284	2.3747	2.261	2.5095	2.4720	2.4060	2.273	2.4764	2.4829	2.4457	2.279	2.4775	2.4413
Cu…O											3.0266	3.205	3.1518	3.2303	3.1946	3.151	3.3095	3.2914	3.1961	3.257	3.3563	3.2138
N_1-Cu-N_2	77.15	82.42	83.30	77.50	80.1	83.65	77.37	77.64	83.84	77.32	77.76	80.83	82.69	83.63	77.81	80.88	83.38	83.71	78.67	80.51	83.51	78.47
P_1-Cu-P_2	124.73	106.16	108.31	125.93	122.7	113.28	125.08	125.83	112.56	125.76	115.75	110.81	102.90	105.69	113.92	116.44	103.86	105.57	117.97	112.91	103.64	118.95
N_1-Cu-P_1	106.48	97.49	98.60	111.57	111.4	123.72	111.73	110.59	122.61	110.90	113.72	109.09	139.21	136.25	120.30	121.45	123.93	124.10	120.77	121.44	121.55	119.84
N_1-Cu-P_2	113.63	138.45	136.46	109.96	109.4	105.31	110.47	110.44	106.99	110.47	119.25	125.75	99.39	99.35	113.80	109.98	112.12	111.11	107.87	105.44	113.62	108.73
N_2-Cu-P_1	115.64	137.48	136.36	109.96	106.4	105.29	110.47	108.76	103.82	109.08	113.80	118.37	98.05	100.02	107.75	107.74	99.04	100.08	117.02	121.75	97.61	116.03
N_2-Cu-P_2	109.26	101.01	98.75	111.57	119.0	123.80	111.73	113.32	125.52	112.95	110.64	108.11	143.94	137.85	118.47	115.24	136.42	133.64	107.77	105.44	138.17	107.58
C_1-O-C_2											121.09	116.91	120.92	119.74	121.86	120.96	122.24	122.08	120.53	121.33	122.42	120.16
DHA	84.28	56.41	57.84	88.64		74.81	88.95	88.05	74.63	88.20	86.39	88.36	52.46	57.98	82.45	82.33	69.03	70.23	88.89	78.80	69.59	89.38

[a] Reference [12], [b] Reference [13].

Table 2. Negative value of the HOMO ($-\varepsilon_{HOMO}$) and LUMO ($-\varepsilon_{LUMO}$) Energies, HOMO-LUMO Gaps Calculated by DFT, and the Lowest Singlet Excited Energies (E_{S1}) Calculated by TDDFT in eV for these Complexes

	$-\varepsilon_{HOMO}$	$-\varepsilon_{LUMO}$	Δ_{H-L}	E_{S1}
$[Cu(phen)(PPh_3)_2]^+$	7.99	4.42	3.57	2.97
$[Cu(dmp)(PPh_3)_2]^+$	8.00	4.28	3.72	3.14
$[Cu(dbp)(PPh_3)_2]^+$	7.97	4.19	3.78	3.17
$[Cu(phen)(POP)]^+$	7.84	4.38	3.46	2.87
$[Cu(dmp)(POP)]^+$	7.84	4.22	3.62	3.02
$[Cu(dbp)(POP)]^+$	7.89	4.13	3.76	3.14

Table 3. Absorption Spectra Obtained by TDDFT Method in Solvent DCM for these Complexes, Together with Experimental Values

	Electronic transitions	λ^{abs}_{max} (nm)	f	Excitation energies (eV)	Main configurations	
$[Cu(phen)(PPh_3)_2]^+$	$S_0 \rightarrow S_1$	390.5	0.0637	3.18	HOMO→LUMO	0.68
					HOMO-2→LUMO	0.17
	$S_0 \rightarrow S_4$	362.1/370[a]	0.0125	3.42	HOMO-1→LUMO	0.67
					HOMO-2→LUMO	0.14
$[Cu(dmp)(PPh_3)_2]^+$	$S_0 \rightarrow S_1$	376.7	0.0621	3.29	HOMO→LUMO	0.70
	$S_0 \rightarrow S_3$	355.9/365[a]	0.0101	3.48	HOMO-1→LUMO	0.67
					HOMO-2→LUMO	0.19
$[Cu(dbp)(PPh_3)_2]^+$	$S_0 \rightarrow S_1$	378.6	0.0567	3.28	HOMO→LUMO	0.69
					HOMO-2→LUMO	-0.12
	$S_0 \rightarrow S_3$	356.3	0.0109	3.48	HOMO-1→LUMO	0.69
$[Cu(phen)(POP)]^+$	$S_0 \rightarrow S_1$	403.8/391[a]	0.0848	3.07	HOMO→LUMO	0.69
					HOMO-2→LUMO	0.14
$[Cu(dmp)(POP)]^+$	$S_0 \rightarrow S_1$	393.8/383[a]	0.0614	3.15	HOMO→LUMO	0.69
$[Cu(dbp)(POP)]^+$	$S_0 \rightarrow S_1$	383.8/378[a]	0.0574	3.23	HOMO→LUMO	0.68
					HOMO-2→LUMO	-0.17

[a] Measured in DCM in reference [13].

Table 4. Emission Spectra Obtained by TDDFT Method in Solvent DCM for these Complexes, Together with Experimental Values

	Electronic transitions	λ^{em} (nm)	Excitation energies (eV)	Main configurations	
$[Cu(phen)(PPh_3)_2]^+$	$T_1 \rightarrow S_0$	752.2/680[a]	1.65	HOMO→LUMO	0.69
$[Cu(dmp)(PPh_3)_2]^+$	$T_1 \rightarrow S_0$	603.1/560[a]	2.06	HOMO-1→LUMO	0.56
				HOMO→LUMO	-0.40
$[Cu(dbp)(PPh_3)_2]^+$	$T_1 \rightarrow S_0$	604.5	2.05	HOMO-1→LUMO	0.53

				HOMO→LUMO	-0.42
$[Cu(phen)(POP)]^+$	$T_1 \rightarrow S_0$	746.4/700[a]	1.66	HOMO→LUMO	0.69
$[Cu(dmp)(POP)]^+$	$T_1 \rightarrow S_0$	623.3/570[a]	1.99	HOMO→LUMO	0.68
$[Cu(dbp)(POP)]^+$	$T_1 \rightarrow S_0$	607.0/560[a]	2.04	HOMO-1→LUMO	0.46
				HOMO→LUMO	0.40
				HOMO-2→LUMO	0.26

[a] Measured in DCM in reference [13].

Table 5. 0-0 and Vertical ($T_1 \rightarrow S_0$) Transition Energies of these Complexes Obtained from DFT, Together with Experimental Values

	0-0	E_{vert} (eV)	Emission maximum (eV) [a]exp	$^a\Phi_p$
$[Cu(phen)(PPh_3)_2]^+$	2.40	1.82	1.82	0.0007
$[Cu(dmp)(PPh_3)_2]^+$	2.63	2.35	2.21	0.0014
$[Cu(dbp)(PPh_3)_2]^+$	2.62	2.35		
$[Cu(phen)(POP)]^+$	2.47	1.86	1.77	0.0018
$[Cu(dmp)(POP)]^+$	2.63	2.21	2.18	0.15
$[Cu(dbp)(POP)]^+$	2.61	2.33	2.21	0.16

[a] Measured in DCM in reference [13].

Table 6. IPs, EAs, Extraction Potentials, and Reorganization Energies for Each Complex (eV)

	IP(v)	IP(a)	HEP	EA(v)	EA(a)	EEP	λ_{hole}	$\lambda_{electron}$
$[Cu(phen)(PPh_3)_2]^+$	9.06	8.71	8.34	3.04	3.34	3.51	0.72	0.47
$[Cu(dmp)(PPh_3)_2]^+$	9.05	8.79	8.51	2.95	3.16	3.37	0.54	0.42
$[Cu(dbp)(PPh_3)_2]^+$	9.00	8.76	8.51	2.91	3.12	3.32	0.49	0.41
$[Cu(phen)(POP)]^+$	8.92	8.60	8.27	2.99	3.19	3.40	0.65	0.41
$[Cu(dmp)(POP)]^+$	8.92	8.66	8.41	2.88	3.15	3.36	0.51	0.48
$[Cu(dbp)(POP)]^+$	8.95	8.66	8.38	2.83	3.06	3.32	0.57	0.49